

Moving Forward to Real-time Imaging-based Monitoring of Cerebrovascular Diseases Using a Microwave Device: Numerical and Experimental Validation

*Original*

Moving Forward to Real-time Imaging-based Monitoring of Cerebrovascular Diseases Using a Microwave Device: Numerical and Experimental Validation / Rodriguez-Duarte, D. O.; Tobon Vasquez, J. A.; Vipiana, F.. - ELETTRONICO. - (2022), pp. 1-4. (Intervento presentato al convegno 3rd URSI Atlantic and Asia Pacific Radio Science Meeting, AT-AP-RASC 2022 tenutosi a Gran Canaria, Spain nel 30 May 2022 - 04 June 2022) [10.23919/AT-AP-RASC54737.2022.9814318].

*Availability:*

This version is available at: 11583/2982066 since: 2023-09-12T23:50:33Z

*Publisher:*

IEEE

*Published*

DOI:10.23919/AT-AP-RASC54737.2022.9814318

*Terms of use:*

This article is made available under terms and conditions as specified in the corresponding bibliographic description in the repository

*Publisher copyright*

IEEE postprint/Author's Accepted Manuscript

©2022 IEEE. Personal use of this material is permitted. Permission from IEEE must be obtained for all other uses, in any current or future media, including reprinting/republishing this material for advertising or promotional purposes, creating new collecting works, for resale or lists, or reuse of any copyrighted component of this work in other works.

(Article begins on next page)



## Moving Forward to Real-time Imaging-based Monitoring of Cerebrovascular Diseases Using a Microwave Device: Numerical and Experimental Validation

D. O. Rodriguez-Duarte\*, J. A. Tobon Vasquez, and F. Vipiana  
 Dept. Electronics and Telecommunications, Politecnico di Torino, Torino, Italy,  
 {david.rodriguez, jorge.tobon, francesca.vipiana}@polito.it

### 1 Introduction

The brain is an organ that requires constant nourishment and high oxygenation, being critically susceptible to the lack of the latter. The deprivation or alteration of the regular supply of oxygen-rich blood temporarily or permanently causes brain cell demise at a rate of millions per minute, provoking variable-term cognitive and physical disabilities and even the patient's death. These disorders are named cerebrovascular diseases and classified within the ischemic and hemorrhagic stroke pathologies [1]. A total or partial artery obstruction (vessel narrowing, clots, or embolism) induces an ischemic-affected area, and blood vessel ruptures cause internal bleeding that forms the hemorrhage within the brain [2, 3]. Regardless of the stroke typology, it is a critical condition and is primordial to receive a prompt diagnosis, medical care, and continuous post-event physiological monitoring, especially during the first few hours after the stroke onset, mitigating its impact and enhancing the rehab rate. In such a framework, clinicians generally support their intervention with imaging-based technologies such as magnetic resonance imaging (MRI) and computerized X-ray tomography (CT), which provide highly reliable images, essentials for stroke condition assessment. However, the stroke management protocols traditionally reserve the utilization of MRI and CT for initial diagnostic and non-continuous follow-up assessments due to their intrinsic constraint regarding time-consume, portability, cost-efficiency, and the ionizing radiation's harmfulness in the case of CT [4].

The limitations of current technologies and the positive effect of a continuous post-event follow-up on medical treatment have motivated the industry and academy to explore complementary brain stroke imaging alternatives such as microwave devices [5, 6, 7, 8, 9, 10, 11, 12, 13]. This approach exploits the existing electric contrast (permittivity and conductivity) between healthy brain tissues and stroke-affected tissues to map the electromagnetic tissue variations via the proper process of generated scattered field and the solution of an inverse scattering problem. Moreover, microwave technology does not use ionizing radiation, being safe for repeated examinations, and allows designing portable, relatively low-cost devices compared to MRI and CT.

In this extended abstract, the authors move forward to a clinical device, presenting the numerical and experimental validation of a compact, low-complexity, and functional prototype for real-time brain stroke monitoring that retrieves 3-D injury mappings. The prototype improves its portability and complexity, reducing its overall dimensions and weight employing only 22 custom-made and low-profile flexible antennas, compared to [10, 11], previously presented by the authors. Moreover, the dynamic monitoring capability validation uses a realistic emulated, numerically and experimentally, hemorrhagic stroke with a variation from 5 to 15 cm<sup>3</sup>, taking a CT scan as a starting point to determine the stroke shape and size. While the numerical head model considers both a single average and a multi-tissue one, the experimental head phantom consists of a single-cavity one.

### 2 Materials and Methods

#### 2.1 Imaging Background

To retrieve a real-time constant mapping of the electrical variation, i.e., the pathology status evolution, we employ a differential scheme that uses the scattering difference ( $\Delta S$ ), occurring during the interval of interest  $[t_0, t_1]$ , with the same approach as in [11]. Then, the output map is stated as  $\Delta \chi = (\epsilon(t_1) - \epsilon(t_0)) / \epsilon_b$ , where  $\epsilon(t_0)$  and  $\epsilon(t_1)$  are the complex permittivities, and  $b$  stands for the background. It relates with the input as

$$\Delta S(t_0, t_1) = -\frac{j \omega \epsilon_b}{2 a_p a_q} \int_D \mathbf{E}_p(t_0) \cdot \mathbf{E}_q(t_0) \Delta \chi \, d\mathbf{r}, \quad (1)$$

assuming a concentrated and weak contrast perturbation, and then applying the Born approximation. In 1, the symbol “ $\cdot$ ” denotes the dot product between vectors,  $j$  is the imaginary unit,  $\omega = 2\pi f$  is the angular frequency, and  $a_p$  and  $a_q$  are the known incoming root-power waves at the  $p$  and  $q$  antenna ports, respectively [14].  $\mathbf{E}_p(t_0)$  and  $\mathbf{E}_q(t_0)$  stand for a reference electric field, i.e., the field in the forecast nominal condition radiated by the  $p$ -th and  $q$ -th antennas. These fields are computed via full-wave simulation of a virtual twin, employing an in-house Finite Element Method EM solver [15] and 3-D realistic models of the antennas and the head.

$$\Delta\chi = \sum_{n=1}^T \frac{1}{\sigma_n} \langle \Delta S, u_n \rangle v_n, \quad (2)$$

Equation 1 is inverted and regularized via the truncated singular value decomposition (TSVD) scheme [16], as shown in Eq. 2, where  $\langle u, \sigma, v \rangle$  is the SVD of the discretized counterpart of the integral operator and  $T$  is the truncation index that acts as a regularizer, it set as -25 dB. Here it is also worthy highly, that though the the building and decomposition of imaging operator is the most computationally expensive part of the procedure, it is just performed once offline. Thus, the real-time monitoring relies mainly in the projection of the differential S-parameters on the pre-computed operator. Finally, the output qualitative description is given by the normalized modulus of the retrieved differential contrast.

## 2.2 Scanner Prototype and Validation Setup

The microwave imaging (MWI) device presented here consists mainly of three elements. A 2-port Vector Network Analyzer(VNA)[17] generates the impinging stimulus and measures the reflection and transmission parameters, a compact and flexible 22-antenna array where each acts as transmitter and receiver, and an electro-mechanical switching matrix, previously reported in [10, 11], that multiplexes the signal from the VNA port to the antenna ports. The VNA is set with -5 dBm and the intermediate filter (IF) to 100 Hz, reaching a measure time per set of about 5 minutes, limited mainly by the switching speed. Though, it can be significantly reduced using solid state switches instead [18]. The antenna system is new version inspired and based on the brick-shaped antenna in [19] and the rigorous layout design process described in [20]. The optimized radiating elements work in a  $-10$  dB band from 0.85 to 1.25GHz in human head proximity, and is made of two staked dielectrically customizable stratus produced with urethane rubber and graphite powder mixture. The first stratus, made of G35(35% Graphite,  $\epsilon_r = 18$ ,  $\sigma = 0.3$ [S/m] at 1 GHz), acts as the monopole substrate, holding the ground plane and the triangular radiator on each side, both printed on flexible commercial 50  $\mu\text{m}$ -thickness polyimide film. The second one, made of G25( $\epsilon_r = 13$ ,  $\sigma = 0.18$ [S/m] at 1 GHz), is a matching medium instead. The Fig. 1(a-c) depicts the implemented system and the antennas.

The system numerically and experimentally approaches a hemorrhagic dynamic stroke condition for validation, using realistic stroke and head models, abstracted from medical images, and an imaging kernel based on an average head model. The stroke considers three states, 5  $\text{cm}^3$ , 10  $\text{cm}^3$  and 15  $\text{cm}^3$ , and is placed around the occipital and parietal zone of the brain, back-part of the head, as shown in Fig. 2. In the numerical assessment, the mimic situation initially considers a uniformly filled head with an average brain, and later a multi-tissue that contains skin, fat, skull, cerebrovascular fluid(CSF), ventricle, gray matter, white matter and cerebellum, as in [22]. On the other hand, the experimental validation considers just the averaged-head approach. In this case, the head is an anthropomorphic single-cavity 3-D printed phantom made of clear resin, which supports the antenna array and

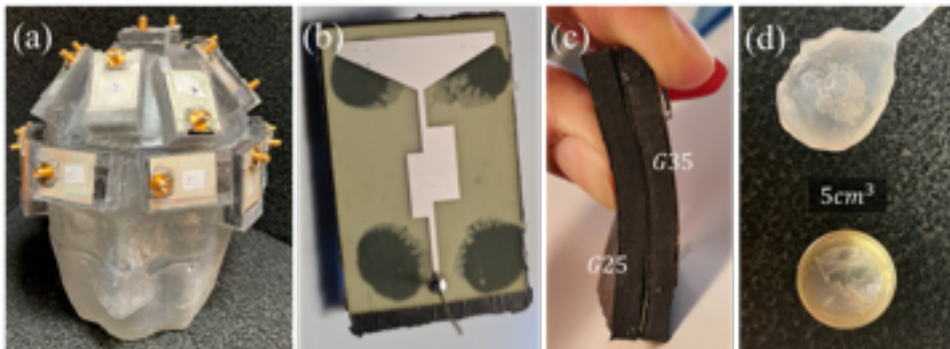


**Figure 1.** Implemented 22-antenna MWI prototype. (a) 3-D printed single cavity head phantom with antenna array wear on top; (b-c) Flexible monopole antenna; (d) non-static stroke phantom.

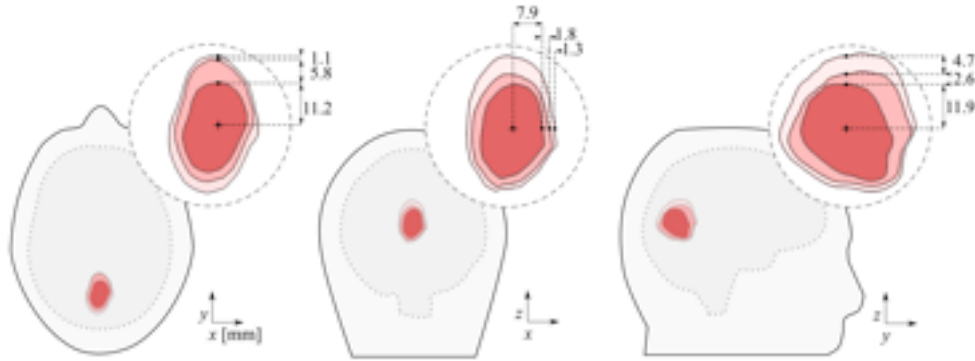


**Figure 2.** Diagram of the modeled evolving stroke condition considering 5, 10 and 15 cm<sup>3</sup> volumetric variations. From left-to-right: transverse, frontal and sagittal plane view. Dimensions in [mm].

contains the average liquid mimicking the brain[21]. Moreover, the stroke is mimicked using a custom homemade balloon filled up through a syringe with a liquid mimicking the blood (see Fig. 1(d)).

### 3 Monitoring Validation

As aforementioned, three differential cases consider the spatial extend variation of a hemorrhagic stroke at different instants. In each case, we take as reference the healthy state measured at  $t_0$ , i.e., the non-stroke numerically and empty stroke experimentally, and then the scattering matrix taken at  $t_1, t_2$  and  $t_3$  with 5, 10, 15 cm<sup>3</sup> stroke volume, respectively. Starting with the simulated scenarios, Fig. 3 and Fig. 4, and the experimental one, Fig. 5, the bellow figures depict the retrieved dielectric contrast normalized at its maximum value. The top row shows a 3-D view indicating the values above -3 dB, while the bottom is a zoom-up transverse plane view around the stroke zone. Moreover, the red circles (center at the maximum of each scenario) denote the contour corresponding respectively to spheres of volume 5, 10 and 15 cm<sup>3</sup> and radii 10.6, 13.7 and 15.3 mm.

The illustrated results demonstrate the system's capability to localize and estimate the shape and size of the stroke targets, with a relatively low error in all studied cases. Also, the retrieved variation appears to follow the shape changes quasi-instantaneously. The simulated cases present a more notable variation in the vertical axes of the transverse view, as expected from the model. In the experimental one, controlling precisely the growing direction of the stroke is challenging, though the results indicate the actual direction accurately.

### 4 Conclusion and Perspectives

This paper presents the numerical and experimental validation of a compact and modular microwave scanner for brain stroke imaging, optimized to work with just a 22-elements array of custom-made flexible antennas. The outcomes demonstrate that the system can retrieve important medical parameters' location and shape under different complex scenarios, but most importantly, a promising capability to follow a real-time evolving condition. However, this preliminary exploration also glimpses the limitations that might cause the lack of a-priori information in the imaging kernel and the non-calibrated error during the measuring, provoking undesired artifacts. For future work, we plan to extend the validation using complex scenarios and approach the identified limitations.

### 5 Acknowledgements

This work was supported by the European Union's Horizon 2020 Research and Innovation Program under the EMERALD project, Marie Skłodowska-Curie grant agreement No. 764479.

### References

- [1] G.A. Donnan, M. Fisher, M. Macleod, and S.M. Davis, "Stroke," *The Lancet*, **371**, no. 9624, pp. 1612–1623, 2008.
- [2] D. Purves, G.J. Augustine, D. Fitzpatrick, et al., editors. "The Blood Supply of the Brain and Spinal Cord.," *Neuroscience*, Sunderland (MA): Sinauer Associates, 2001

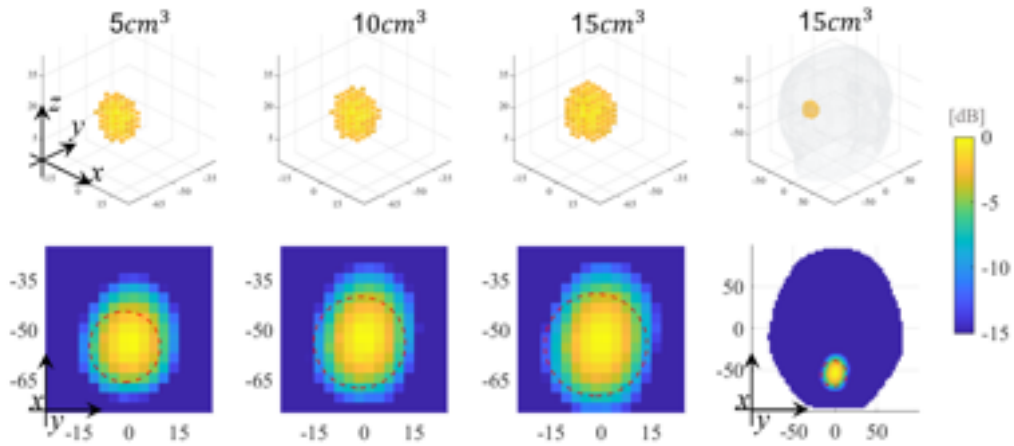


**Figure 3.** Amplitude values of the retrieved dielectric contrast normalized and at its maximum value for the numerical validation using an single-tissue average head. Top row: 3-D view indicating the values above -3 dB. From left-to-right: 0-5 cm<sup>3</sup>, 0-10 cm<sup>3</sup>, 0-15 cm<sup>3</sup>.

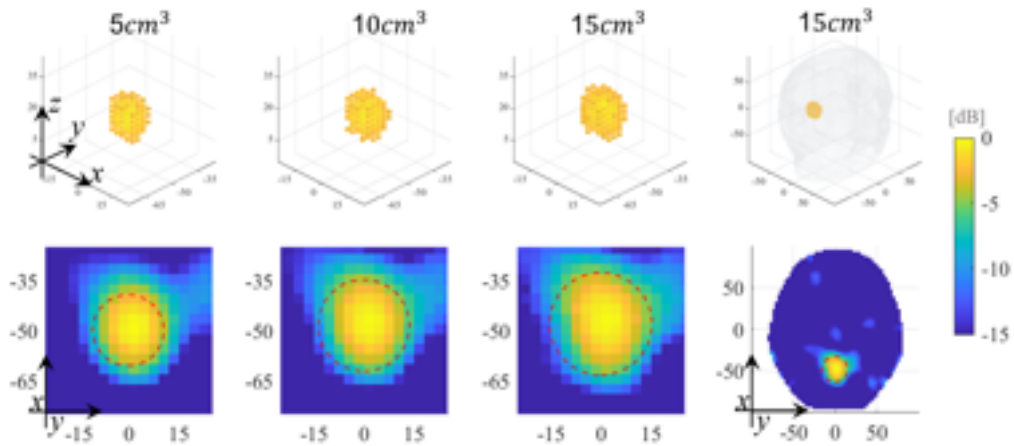


**Figure 4.** Amplitude values of the retrieved dielectric contrast normalized and at its maximum value for the numerical validation using an multi-tissue head. Top row: 3-D view indicating the values above -3 dB. From left-to-right: 0-5 cm<sup>3</sup>, 0-10 cm<sup>3</sup>, 0-15 cm<sup>3</sup>.

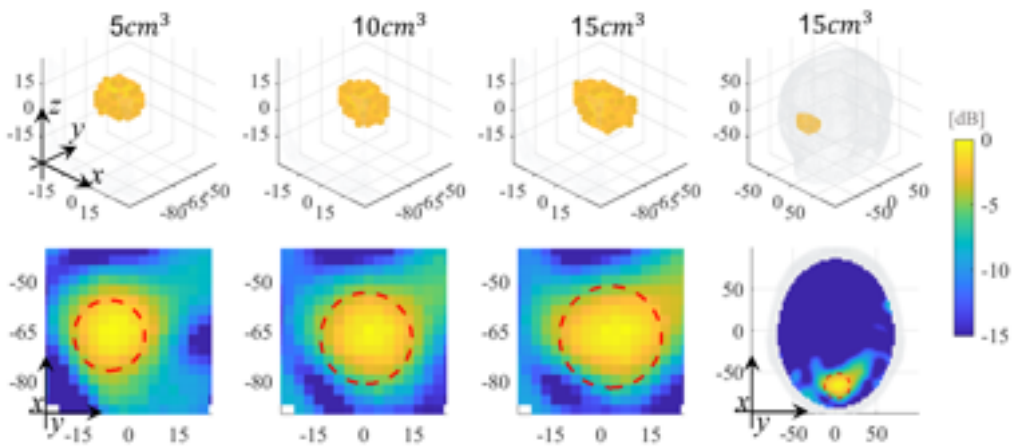


**Figure 5.** Amplitude values of the retrieved dielectric contrast normalized and at its maximum value for the experimental validation using an single-tissue average head. Top row: 3-D view indicating the values above -3 dB. From left-to-right: 0-5 cm<sup>3</sup>, 0-10 cm<sup>3</sup>, 0-15 cm<sup>3</sup>.

- [3] A. Ciccone, M.G. Celani, R. Chiaramonte, C. Rossi and E. Righetti, “Continuous versus intermittent physiological monitoring for acute stroke,” *Cochrane Database of Systematic Reviews* 2013, **5**, no. CD008444, doi:10.1002/14651858.CD008444.pub2
- [4] L. Crocco, I. Karanasiou, M. James, R. Conceição (eds), *Emerging Electromagnetic Technologies for Brain Diseases Diagnostics, Monitoring and Therapy*. Springer, 2018
- [5] S. Candefjord, J. Winges, A. Malik, Y. Yu, T. Rylander, T. McKelvey, A. Fhager, M. Elam, and M. Persson, “Microwave technology for detecting traumatic intracranial bleedings: tests on phantom of subdural hematoma and numerical simulations,” *Med. & Biol. Eng. & Comput.*, **55**, August 2017, pp. 1177–1188, doi: 10.1007/s11517-016-1578-6
- [6] A. Fhager, S. Candefjord, M. Elam, and M. Persson, “Microwave diagnostics ahead: Saving time and the lives of trauma and stroke patients,” *IEEE Microwave Mag.*, **19**, 3, May 2018, pp. 78–90, doi: 10.1109/MMM.2018.2801646.
- [7] I. Merunka, A. Massa, D. Vrba, O. Fiser, M. Salucci, and J. Vrba, “Microwave tomography system for methodical testing of human brain stroke detection approaches,” *Int. J. of Antennas Propag.*, **2019**, no. Article ID 4074862, March 2019, pp. 1–9, doi: 10.1155/2019/4074862.
- [8] A. Fedeli, C. Estatico, M. Pastorino, and A. Randazzo, “Microwave detection of brain injuries by means of a hybrid imaging method,” *IEEE Open Journal of Antennas and Propagation*, **1**, September 2020, pp. 513–523, doi: 10.1109/OJAP.2020.3024276.
- [9] A. S. M. Alqadami, N. Nguyen-Trong, B. Mohammed, A. E. Stancombe, M. T. Heitzmann, and A. Abbosh, “Compact unidirectional conformal antenna based on flexible high-permittivity custom-made substrate for wearable wideband electromagnetic head imaging system,” *IEEE Transactions on Antennas and Propagation*, **68**, 1, January 2020, pp. 183–194, doi: 10.1109/TAP.2019.2938849
- [10] J. A. Tobon Vasquez, R. Scapatucci, G. Turvani, G. Bellizzi, D. O. Rodriguez-Duarte, N. Joachimowicz, B. Duchene, E. Tedeschi, M. R. Casu, L. Crocco, and F. Vipiana, “A prototype microwave system for 3D brain stroke imaging,” *SENSORS*, **20**, no. Article ID 9, 2607, May 2020, pp. 1–16, doi: 10.3390/s20092607
- [11] D. O. Rodriguez-Duarte, J. A. Tobon Vasquez, R. Scapatucci, G. Turvani, M. Cavagnaro, M. R. Casu, L. Crocco, and F. Vipiana, “Experimental Validation of a Microwave System for Brain Stroke 3-D Imaging,” *Diagnostics*, **11**, no. Article ID 1232, 2607, July 2021, pp. 1–18, doi: 10.3390/diagnostics11071232
- [12] L. Guo, M. K. Farsani, A. Stancombe, K. Bialkowski and A. Abbosh, “Adaptive Clustering Distorted Born Iterative Method for Microwave Brain Tomography with Stroke Detection and Classification,” *IEEE Transactions on Biomedical Engineering*, doi: 10.1109/TBME.2021.3122113.
- [13] N. Ghavami, et al., “The Use of Metasurfaces to Enhance Microwave Imaging: Experimental Validation for Tomographic and Radar-Based Algorithms,” *IEEE Open Journal of Antennas and Propagation*, **3**, January 2022, pp. 89–100, doi: 10.1109/OJAP.2021.3135146.
- [14] N. K. Nikolova, *Introduction to Microwave Imaging*. Cambridge: Cambridge University Press, 2017.
- [15] E. A. Attardo, A. Borsic, G. Vecchi and P. M. Meaney, “Whole-System Electromagnetic Modeling for Microwave Tomography,” *IEEE Antennas and Wireless Propagation Letters*, **11**, pp. 1618-1621, 2012, doi: 10.1109/LAWP.2013.2237745.
- [16] M. Bertero and P. Boccacci, *Introduction to Inverse Problems in Imaging*. Inst. Phys., Bristol, U.K., 1998.
- [17] Keysight Technologies. Keysight Streamline Series USB Vector Network Analyzer P937XA 2-port, up to 26.5 GHz. *Data Sheet Tech. Specif.* 2018.
- [18] I. Sarwar, G. Turvani, M. R. Casu, J. A. Tobon Vasquez, F. Vipiana, R. Scapatucci, and L. Crocco, “Low-cost low-power acceleration of a microwave imaging algorithm for brain stroke monitoring,” *J. Low Power Electron.s Appl.*, **8**, 4, no. Article ID 43, November 2018, pp. 1–13, doi: 10.3390/jlpea8040043
- [19] D. O. Rodriguez-Duarte, J. A. Tobon Vasquez, R. Scapatucci, L. Crocco and F. Vipiana, “Brick Shaped Antenna Module for Microwave Brain Imaging Systems,” *IEEE Antennas and Wireless Propagation Letters*, **19**, 12, December 2020, pp. 2057–2061, doi: 10.1109/LAWP.2020.3022161.

- [20] R. Scapatucci, J. A. Tobon Vasquez, G. Bellizzi, F. Vipiana and L. Crocco, "Design and Numerical Characterization of a Low-Complexity Microwave Device for Brain Stroke Monitoring," *IEEE Transactions on Antennas and Propagation*, **66**, 12, December 2018, pp. 7328–7338, doi: 10.1109/TAP.2018.2871266.
- [21] N. Joachimowicz, B. Duchene, C. Conessa, and O. Meyer, "Anthropomorphic breast and head phantoms for microwave imaging," *Diagnostics*, vol. 85, pp. 1–12, Dec. 2018.
- [22] D. O. Rodriguez-Duarte, J. A. Tobon Vasquez, R. Scapatucci, L. Crocco and F. Vipiana, "Assessing a Microwave Imaging System for Brain Stroke Monitoring via High Fidelity Numerical Modelling," *IEEE Journal of Electromagnetics, RF and Microwaves in Medicine and Biology*, 2021, doi: 10.1109/JERM.2020.3049071.